Reconfiguration strategy for a DC-DC boost converter using sliding mode observers and fault identification with a neural network ⋆

Diego S. Carneiro * **Lucas Jonys R. Silva** * **Flávio A. Faria** **
Rafael F. Q. Magossi *** **Vilma A. Oliveira** *

* *Escola de Engenharia de São Carlos, Universidade de São Paulo, SP (e-mail: diegocarneiro@usp.br, lucasjonys@usp.br,voliveira@usp.br).*
** *Universidade Estadual Paulista (Unesp), Faculdade de Engenharia, Ilha Solteira, SP (e-mail: flavio.faria@unesp.br)*
*** *Centro Federal de Educação Tecnológica Celso Suckow da Fonseca, CEFET em Nova Friburgo, RJ (e-mail: rafael.magossi@cefet-rj.br).*

Abstract: In this paper, a method for the reconfiguration of the operation of DC-DC boost converters is proposed using sliding mode observers (SMOs). Open and high gain sensor faults are analyzed. The reconfiguration strategy involves mainly a fault detection and identification stages. In the fault detection stage, a SMO is designed for generating a residual and in the fault identification stage, an algorithm using neural network with pattern recognition is proposed. Two auxiliary SMO are used to estimate the sensor outputs to provide a proper feedback signal to keep the system stable in case of occurrence of fault. Simulation results of a DC-DC boost converter in the presence of faults illustrate the efficiency of reconfiguration strategy.

Keywords: DC-DC converters, sensor faults, sliding mode control, sliding mode observer, pattern recognition.

1. INTRODUCTION

The increasing interest in DC microgrids emerges from the growing use of renewable energy sources and, in general, the DC-DC converters are employed since they may guarantee maximum energy extraction, as well as adequate levels of voltage/current from the main power supply (Chaturvedi et al., 2021; Magossi et al., 2021). For instance, in photovoltaic systems the output voltage of the photovoltaic arrays needs to be increased in order to be connected to the grid (Vázquez et al., 2013). There are several topologies of DC-DC converters in the literature which can provide output voltage greater than input, and among them, the boost converter has a simple structure (Ivanovic et al., 2014; Magossi et al., 2020).

As the DC-DC converters operate in an on-off mode, the sliding mode control (SMC) is an appropriate method for regulating its voltage and current, allowing a natural way of control by combining the converter state variables in its operating modes (Utkin, 2013; Martinez-Treviño et al., 2019). Furthermore, the SMC technique is very attractive due to its robustness in relation to parametric uncertainties and simplicity in its design (Yazici and Yaylaci, 2016; Komurcugil et al., 2020).

Although DC–DC converters may operate with robust controllers, they are commonly used in practical environments with harsh conditions and are likely to be damaged, moreover, in many industrial applications the power interruption is not tolerated since it affects not only the maintenance cost but also the operational cost, thus reliability and failure analysis for DC–DC converters are critical to making reliable products (Yao et al., 2013; Ferreira Costa and Liserre, 2018; Tarzamni et al., 2021). There are several works in the literature enhancing the reliability of DC-DC converters, such as in Li et al. (2019) where a sliding mode observer (SMO) for sensor faults detection in a buck boost converter is proposed. A method for sensor fault detection and reconfiguration for a boost converter is proposed by Li et al. (2018) using a state observer for fault detection. Silveira and Araújo (2020) proposes a fuzzy logic based scheme for faults in voltage and current sensor, switch and capacitor for DC-DC converters.

Methods for fault detection and isolation of actuator's fault in DC-DC converters can be seen in Espinoza-Trejo et al. (2016), Givi et al. (2017). In Bento and Cardoso (2018) a comprehensive survey for general techniques for fault diagnosis of open circuit and short-circuit is presented.

In this work, a reconfiguration strategy for a DC-DC boost converter considering current and voltage sensors faults is proposed. A pattern recognition with a neural network was developed to identify the type of fault. This approach can be also used as a framework to detect actuator and component faults for similar DC-DC converters. The

⋆ This research was supported by CNPq - Conselho Nacional de Pesquisa, Brazil, under grant 305892/2017-7, by FAPESP - Fundação de Amparo à Pesquisa do Estado de São Paulo, SP, Brazil, under grants 2014/50851-0 and 2019/25530-9 and by CAPES - Coordenação de Aperfeiçoamento de Pessoal de Nível Superior, Brazil, with Finance Code 001 under grant 88887.505861/2020-00.

contribution of this work is on the identification of the class of faults and on the reconfiguration strategy which is based on the change of the estimates of current or voltage depending on the type of sensor fault.

Following this introduction, in Section II, the boost DC-DC converter control and observer based on the sliding mode technique are described. In Section III, the proposed identification method and the reconfiguration strategy is presented. In Section IV, simulation scenarios with current and voltage sensors faults are checked with and without the reconfiguration strategy. Finally, in Section V, some concluding remarks are presented.

Notation: The augmented system with the sensor fault model error and its estimate are denoted by $\tilde{e}$ and $\hat{\tilde{e}}$, respectively. The inductor current and capacitor voltage estimate are denoted by $\hat{x}_{i_L}$ and $\hat{x}_{v_C}$, respectively. The symbols $||\cdot||$ denote the euclidean norm and in symmetric matrices, $\star$ denotes the transposed element of the matrix, $A \prec 0$ ($A \succ 0$) means that A is a negative (positive) definite matrix and $He(M) = M + M'$.

2. PRELIMINARIES

In this section, results from the literature of SMC and SMO designs for a boost converter are summarized.

2.1 Sliding mode control of DC-DC converters

The operation of a boost DC-DC converter without parasitic resistances can be described by the control input $d(\sigma(t))$ for the off state and for the on state of the active switching device and the circuit equations can be written as:

$$\begin{aligned} \dot{x}(t) &= A_{\sigma(t)}x(t) + b \\ y(t) &= C_{out}x(t) \end{aligned} \tag{1}$$

where

$$x(t) = \begin{bmatrix} i_L(t) \\ v_c(t) \end{bmatrix},\ A_{\sigma(t)} = \begin{bmatrix} \frac{-R}{L} & \frac{-(1-d(\sigma(t)))}{L} \\ \frac{(1-d(\sigma(t)))}{C} & \frac{-1}{R_oC} \end{bmatrix}$$

$$b = \begin{bmatrix} \frac{V_{in}}{L} \\ 0 \end{bmatrix},\ C_{out} = \begin{bmatrix} 1 & 0 \\ 0 & 1 \end{bmatrix}$$

$$d(\sigma(t)) = \begin{cases} 0, & \text{if } \sigma(t) = 1 \\ 1, & \text{if } \sigma(t) = 2 \end{cases} \tag{2}$$

with i_L the inductor current, v_c the output capacitor voltage, L the inductance, C the capacitance, R the inductor resistance, R_o the load resistance, V_{in} the input voltage source (constant).

The SMC project can be divided into two stages. Firstly, it is necessary to define a sliding surface that is attractive for the trajectories of the converter. In the sequence, a switching control law is built such that the state reach the previously established surface and evolve on it until reaching the system equilibrium point (Zhao et al., 2019; Utkin, 2013), in a family of the system equilibrium points given by Deaecto et al. (2010):

$$X_e = -A_\lambda^{-1}b \tag{3}$$

where X_e is from a convex combination of matrices $A_\lambda = \sum_{i=1}^{2} \lambda_i A_i$ with $\sum_{i=1}^{2} \lambda_i = 1$.

The objective of the SMC is to control the output voltage of the converter with zero steady-state error and fast dynamic response. The sliding surface is thus defined by:

$$S = K_g(x(t) - x_e) + \int_0^t K_{int}(x(t) - x_e)\, d\tau. \tag{4}$$

where $K_{int} = [0 \quad K_s]$ and $K_g = [K_i \quad K_v]$. This surface (4) is designed to reach an equilibrium point $x_e = [i_e \quad v_e]' \in X_e$.

The control law must be chosen such that the trajectory reaches the surface S in a finite time and remains there, reaching the desired equilibrium point (Utkin et al., 2020). A continuous component u_{eq} and a discontinuous component u_n form the signal u that yields the duty cycle to generate the converter switch signal via a pulse-width modulation (PWM) technique:

$$u = u_{eq} + u_n. \tag{5}$$

The continuous component acts when the trajectory reaches the surface S, ensuring the movement over it. Therefore, u_{eq} must satisfy the condition $\dot{S} = 0$, being $\dot{S}$ the time derivative of S that can be obtained as:

$$\dot{S} = K_g\dot{x} + K_{int}(x(t) - x_e). \tag{6}$$

Using (1), (6) can be expressed as:

$$\dot{S} = \left[\frac{-K_iR}{L} + \frac{K_v(1 - d(\sigma(t)))}{C}\right] i_L + \left[\frac{K_v}{R_oC} + \frac{K_i(1 - d(\sigma(t)))}{L}\right] v_C. \tag{7}$$

When the steady state is reached, the equivalent control corresponding to the equilibrium point x_e can be calculated making $\dot{S}$ in (7) equal to zero, yielding:

$$u_{eq} = 1 - \frac{R_oLC\,(K_iRi_e - K_iV_{in}) + L^2K_vv_e}{K_vLi_e - K_iCv_e}. \tag{8}$$

The discontinuous component acts by switching between positive and negative values above and below the surface S and can be defined using the signal function $u_n = \text{sign}(S)$.

Finite frequency switching of the control signal leads to undesirable oscillations of finite amplitude, characterizing the phenomenon known as chattering, which reduces the control precision and generates excessive wear on the mechanical components of the converter (Utkin, 2013). However, the implementation of a discontinuous control law by the signal function requires an infinite frequency switching when the trajectory reaches the surface, which is not applicable (Yazici and Yaylaci, 2016).

Thus, a solution to reduce chattering is to use smooth continuous control signals (Shtessel et al., 2014). However, there is a trade-off between reduced chattering and control accuracy. The control law must be adequately smoothed, seeking an appropriate point between control bandwidth and tracking precision (Slotine et al., 1991). A way to smooth the control signal is to use a layer of hysteresis ϵ given by:

$$u_n = \begin{cases} \text{sign}(S), & |S| > \epsilon \\ S/\epsilon, & \text{otherwise} \end{cases} \tag{9}$$

As the SMC control u yields the duty cycle to generate the converter switch signal via a pulse-width modulation

(PWM) technique, the surface gains are selected such that $0 < u_{eq} < 1$ in (8).

2.2 Sensor fault detection and identification

In a standard fault detection, identification and reconfiguration (FDIR) strategy, a residual is generated when the system output differs from an expected value. If this residual is greater than a threshold, an alarm is triggered and a fault is detected. Meanwhile, some reconfiguration techniques require a fault identification, that is, along with detecting the presence of fault, the type of fault and its location estimation can be very important. After fault detection and identification, a decision must be made to reconfigure the system operation by changing the controller input or gain (Hwang et al., 2009).

The fault detection technique used here follows the work of Li et al. (2019) which is based on a sliding mode observer. In this technique, there must be a control law $u(t)$ that leads system (1) to a constant equilibrium state $x_e \in X_e$ when $t \to \infty$. Define the error between the state and the equilibrium state as:

$$e(t) = x(t) - x_e \tag{10}$$

rewrite (1) considering (10), an affine switched error system can be obtained as:

$$\begin{aligned} \dot{e}(t) &= A_{\sigma(t)}e(t) + k_{\sigma(t)} \\ k_{\sigma(t)} &= A_{\sigma(t)}x_e(t) + b \\ y_e(t) &= C_{out}e(t). \end{aligned} \tag{11}$$

The fault affects the system output directly and system (11) with sensor faults can be described as:

$$\begin{aligned} \dot{e}(t) &= A_{\sigma(t)}e(t) + k_{\sigma(t)} \\ y_{e_f}(t) &= C_{out}e(t) + Df_s(t) \end{aligned} \tag{12}$$

where $f_s(t)$ represents sensor faults and $D = I$ is the sensor fault distribution matrix with appropriate dimensions and $y_{e_f}(t) = y_e(t) + Df_s(t)$. Transforming the sensor fault in a pseudo-actuator fault, a new variable z is defined, and an augmented system is:

$$\begin{aligned} \begin{bmatrix} \dot{e}(t) \\ \dot{z}(t) \end{bmatrix} &= \begin{bmatrix} A_{\sigma(t)} & 0 \\ C_{out} & 0 \end{bmatrix} \begin{bmatrix} e(t) \\ z(t) \end{bmatrix} + \begin{bmatrix} k_{\sigma(t)} \\ 0 \end{bmatrix} + \begin{bmatrix} 0 \\ D \end{bmatrix} f_s(t) \\ \dot{z}(t) &= C_{out}e(t) + Df_s(t). \end{aligned} \tag{13}$$

Since $z = [0 \quad I]\,[e \quad z]'$, the augmented error state vector is defined as $\tilde{e} = [e \quad z]'$ and $\tilde{y}_e = z$. System (13) can be written as:

$$\begin{aligned} \dot{\tilde{e}}(t) &= \tilde{A}_{\sigma(t)}\tilde{e}(t) + \tilde{k}_\sigma(t) + \tilde{D}f_s(t) \\ \tilde{y}_e(t) &= \tilde{C}_{out}\tilde{e}(t) \end{aligned} \tag{14}$$

where

$$\tilde{A}_{\sigma(t)} = \begin{bmatrix} A_{\sigma(t)} & 0 \\ C_{out} & 0 \end{bmatrix}, \tilde{k}_\sigma(t) = \begin{bmatrix} k_{\sigma(t)} \\ 0 \end{bmatrix}, \; \tilde{D} = \begin{bmatrix} 0 \\ D \end{bmatrix}, \quad \tilde{C}_{out} = [\,0 \;\; I\,].$$

A model-based sensor fault observer should be designed to: (1) estimate the plant state from its output measurements in nominal conditions; (2) Produce a fast error between the output and estimated states in fault conditions; (3) Yield stable error dynamic in fault conditions.

From the first requirement, it is reasonable to design an observer with similar dynamics as the plant model, therefore, the fault observer structure is assumed as follows:

$$\begin{aligned} \dot{\hat{\tilde{e}}}(t) &= \tilde{A}_{\sigma(t)}\hat{\tilde{e}}(t) + Ge_y(t) + \tilde{D}\nu \\ \hat{\tilde{y}}_e(t) &= \tilde{C}_{out}\hat{\tilde{e}}(t) \\ e_y(t) &= \tilde{y}_e(t) - \hat{\tilde{y}}_e(t). \end{aligned} \tag{15}$$

Denoting $\bar{e}(t) = \tilde{e}(t) - \hat{\tilde{e}}(t)$, the SMO error is given by:

$$\dot{\bar{e}}(t) = (\tilde{A}_{\sigma(t)} - G\tilde{C}_{out})\bar{e}(t) + \tilde{D}(f_s(t) - \nu) + \tilde{k}_\sigma(t) \tag{16}$$

with the term ν given by a sliding law of the form:

$$\nu = \begin{cases} \rho\frac{Fe_y(t)}{||Fe_y(t)||}, & \text{if } e_y(t) \neq 0 \\ 0, & \text{if } e_y(t) = 0 \end{cases} \tag{17}$$

where ρ is a given constant and matrices G in (16) and F are to be found. The matrix F can be calculated assuming that there exists a matrix $P > 0$, $\mathscr{S}$ that satisfies:

$$\begin{bmatrix} P \\ \mathscr{S}' \end{bmatrix} \tilde{D} = \mathcal{C}'F', \text{ with } \mathcal{C} = \begin{bmatrix} \tilde{C}_{out} & 0_n \end{bmatrix} \tag{18}$$

the matrix F can be found as:

$$F = \tilde{D}' \begin{bmatrix} P \\ \mathscr{S}' \end{bmatrix} \mathcal{C}'. \tag{19}$$

The fault observer must be asymptotically stable in presence of fault and the observed output must differ from the system output in fault situations, generating a residual error signal $\bar{r}(t)$. Assume that the sensor fault is a bounded fault, such that $\|f_s(t)\| < \rho$ and define the residual error as $\bar{r}(t) = e_y - Df_s(t)$. The augmented system for residual error generation is:

$$\begin{aligned} \dot{\bar{e}}(t) &= (\tilde{A}_{\sigma(t)} - G\tilde{C}_{out})\tilde{e}(t) + \tilde{D}(f_s(t) - \nu) + \tilde{k}_\sigma(t) \\ \bar{r}(t) &= \tilde{C}_{out}\bar{e} - \tilde{D}f_s(t). \end{aligned} \tag{20}$$

To deal with the effect of the fault in the error dynamics (16), faults in residual are minimized by a H_∞ performance, such that:

$$\int_0^\infty \bar{r}'(t)\bar{r}(t)dt < \gamma^2 \int_0^\infty f_s(t)'f_s(t)dt. \tag{21}$$

The observer matrix G in (16) and the matrix F of (19) can be obtained by Theorem 1.

Theorem *1.* (Li et al. (2019)). If there exist matrix variables $\mathcal{G}, \mathcal{W}, \mathscr{S}$ and $P \succ 0$ satisfying the inequalities (22), then system (20) is asymptotically stable and guarantees the robust performance (21).

$$\begin{bmatrix} He(P\tilde{A}_\ell - \mathcal{G}) & 0 & P\tilde{k}_\ell + \tilde{A}'_\ell\mathscr{S} - \mathcal{W} & \tilde{C}'_{out} \\ * & -\gamma^2 I & 0 & 0 \\ * & * & 2\tilde{k}'_\ell\mathscr{S} & 0 \\ * & * & * & -I \end{bmatrix} \prec 0 \tag{22}$$

where $\ell = 1, 2$.

When (22) is feasible, $G = P^{-1}\mathcal{G}\tilde{C}'_{out}(\tilde{C}_{out}\tilde{C}'_{out})^{-1}$ is the gain matrix of (16) and F can be found using (19).

3. MAIN RESULTS

A diagram of the FDIR process is presented in Figure 1. To make the system control reconfiguration possible, a sliding mode observer for fault detection was implemented.

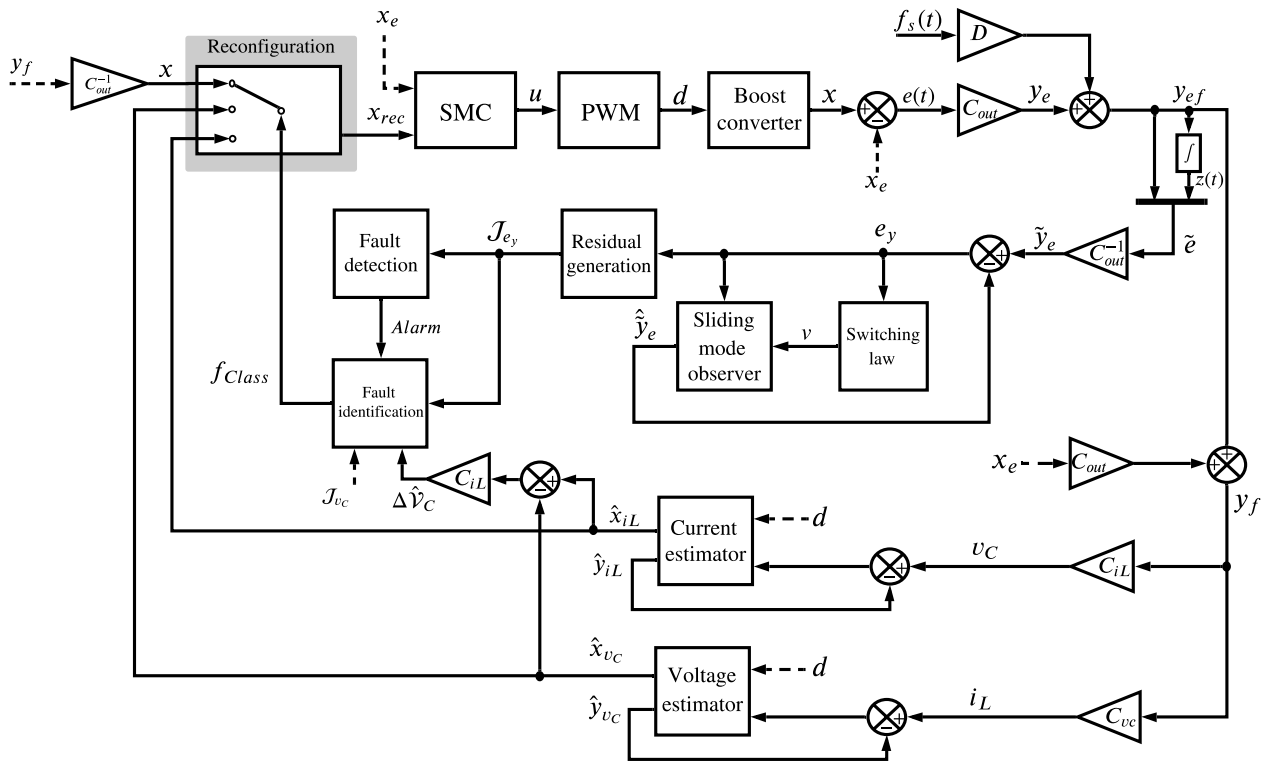

Figure 1. Diagram of fault detection, identification and reconfiguration for the boost DC-DC converter. The switch logic in the reconfiguration box selects the SMC feedback input: current, voltage estimate or the actual plant state.

In the reconfiguration strategy, two state observers were designed for estimating the inductor current and capacitor voltage, denoted by $i_{L_{est}}$ and $v_{C_{est}}$, respectively. Both current and voltage estimators designs follow the structure:

$$\begin{aligned}\dot{\hat{x}}(t) &= A_{\sigma(t)}\hat{x}(t) + b + L_{est}(sign(y_f(t) - \hat{y}(t))) \\ y(t) &= C_{est}\hat{x}(t)\end{aligned} \tag{23}$$

where $y_f(t)$ represents the sensors outputs with the presence of fault, L_{est} is the gain observer, $A_{\sigma(t)}$ and b is the same of the boost converter and $C_{i_L} = [0 \quad I]$ for $i_{L_{est}}$ and $C_{v_C} = [I \quad 0]$ for $v_{C_{est}}$. Note that the current estimator considers only the voltage measurement and the same logic is applied to the voltage estimator. This consideration is very important for the reconfiguration strategy and it will be discussed later on this paper. The matrix L is obtained by considering extremely negative poles in the equation $A_{\sigma(t)} - LC$, because the dynamic of the observers must be faster than the plant.

Since C_{out} of the boost converter is an identity matrix, it is possible to access all system states, that is, the inductor current and capacitor voltage are measured. A reference x_e corresponds to an equilibrium point attainable for a nominal system and it was considered constant. The strategy for the reconfiguration is based on the observer estimates for the current and voltage. The observer input is the equilibrium state, and the feedback signal is changed to the estimate state when fault is detected. The observed estimates are called virtual measurements. To evaluate the residual signal, the function $\mathcal{J}(\cdot)$ is defined:

$$\mathcal{J}(e_y) = \mathcal{J}_{e_y} = \sqrt{\frac{1}{T}\int_{T_0}^{t} e_y(\tau)e_y(\tau)d(\tau)} \tag{24}$$

where T_0 is the initial evaluation time, T is the time step and e_y is obtained through (15). A fault is detected if $\mathcal{J}(e_y) > \mathcal{J}_{th}$ and an alarm flag ($Alarm$) value goes to one, or zero otherwise. A threshold can be defined by:

$$\mathcal{J}_{th} = \sup_{f_s(t)=0} \mathcal{J}(e_y) \tag{25}$$

which corresponds to the maximum $\mathcal{J}(e_y)$ for a no fault test. However, it was noticed that when the system load R_o or source V_{in} values change, which is clearly possible in practical situations, the alarm is takes the value 1, even though there is no fault. A possible strategy to circumvent these false alarms is to increase the threshold. Meanwhile, high values of $\mathcal{J}_{th}$ will make the fault identification slower, leading the system to high values of current or voltage when the sensor signal is incorrect.

3.1 Classification of the sensor faults

A pattern recognition with neural network is an efficient classification method that produce a rapid output and it is a good alternative for fault identification, since the whole classification consists in simple algebraic operations, which is a good advantage comparing to model-based approach in terms of computational efforts.

In this work, two classes of fault are considered: an open sensor fault meaning a null signal in the sensor measurement and a high gain sensor fault corresponding to a large deviation of sensor measurement comparing to nominal conditions. There are two sensors, with two types of fault each resulting in four classes of faults and a class **No fault** in no fault situation, resulting in five classes

(f_{Class}). A representation of these classes can be seen in Table 1.

Table 1. Fault classes

Classes	Number	Label
No fault	1	NOFT
Inductor current sensor open fault	2	ILOP
Inductor current sensor high gain fault	3	ILHG
Capacitor voltage sensor open fault	4	VCOP
Capacitor voltage sensor high gain fault	5	VCHG

In fault identification, the goal is to determine which class belongs the system, given a set of inputs. For this purpose, a multi layer perceptron neural network for pattern recognition (P_{rnn}) was used. The P_{rnn} was designed with the following characteristics: one hidden layer containing four neurons with sigmoid activation functions; one output layer containing five neurons with softmax activation function. The scaled conjugate gradient backpropagation algorithm with the cross entropy performance index was used for training the P_{rnn} with the following parameters: change in weight for second derivative approximation equals to 5×10^{-5}; parameter for regulating the indefiniteness of the Hessian equals to 5×10^{-7}. The samples distribution in the network training, validation and test are given by 70%, 15% and 15%, respectively.

For the data gathering process, some assumptions were made: (a) only one type of fault in one sensor occurs in the time window analyzed; (b) both faults and change in parameters occur in steady state (that is, at the equilibrium point); (c) only changes in R_o or V_{in} are allowed in the time window; (d) parameters changing occurs only before the fault. In the diagram of Figure 2, all the tests executed were described in a tree, such that each branch, from the left to the right, represents a combination in the test. That is, the first level represents one of two sensors, then the type of fault, followed by each parameter that changes in a defined time with the respective value. For high gain faults, two variations were considered.

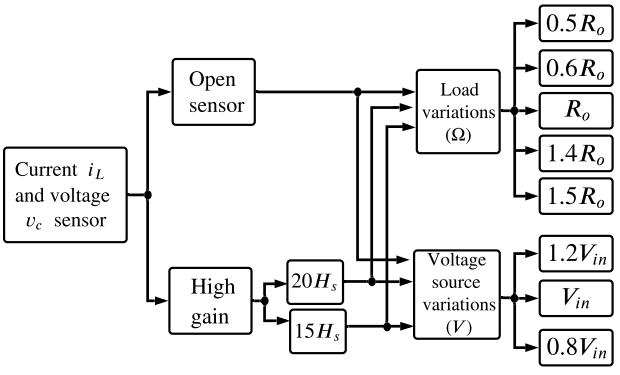

Figure 2. Diagram of simulation cases for the gathered data. H_s is the nominal gain of the sensor.

3.2 FDIR Algorithm

A function of inputs that returns a number in a finite array corresponding to a class of faults can be defined as $P_{rnn}(\cdot)$. For this paper, three inputs were applied: $\mathcal{J}_{e_y}, \mathcal{J}_{v_C}$, and $\Delta\hat{\mathcal{V}}_C$, where $\Delta\hat{\mathcal{V}}_C$ is the error between the capacitor voltage of the current estimator and the voltage estimator, respectively. The fault identification output will be used for reconfiguration only if $Alarm = 1$, otherwise, no reconfiguration strategy is required since there is no fault. According to the $P_{rnn}(\cdot)$ output, a reconfiguration strategy will be enabled selecting the control feedback signal. For the whole FDIR strategy, there are two parallel routines, one is responsible for the fault detection and identification as can be seen in Algorithm (1) and the other for the system reconfiguration (Algorithm (2)).

Algorithm 1 Fault detection and identification

- Initialize: Alarm $= 0$, $\hat{\tilde{y}}_e(0) = 0$

for $t = 0, \ldots, t_{stop}$ **do**
- Augment $e(t)$ into $\tilde{e}$
- Calculate $e_y(t) = \tilde{y}_e(t) - \hat{\tilde{y}}_e(t)$
- Calculate $J = \mathcal{J}_{e_y}, \mathcal{J}_{v_C}, \Delta\mathcal{V}_c$

if $J > J_{th}$ **then**
- $Alarm \leftarrow 1$;
- $f_{Class} \leftarrow P_{rnn}(J, \mathcal{J}_{v_C}, \Delta\mathcal{V}_c)$
- Call(Algorithm 2)

else
- $Alarm \leftarrow 0$;

end if

end for

Algorithm 2 Reconfiguration

if $\hat{i}_{L_1} > 50 + i_e$ & $f_{Class} = 1$ **then**
- $x_{reconfig}(t) \leftarrow \hat{x}_{i_L}(t)$

else

switch f_{Class} **do**

case 1
- $x_{reconfig}(t) \leftarrow x(t)$

case 2, 3
- $x_{reconfig}(t) \leftarrow \hat{x}_{i_L}(t)$

case 4, 5
- $x_{reconfig}(t) \leftarrow \hat{x}_{v_C}(t)$

end if

Remark: Note that in the reconfiguration algorithm there is a comparison with $\hat{i}_{L_1}$ and a value of $50 + i_e$. It means that if the inductor current exceeds 50A from its equilibrium point and the Alarm goes on, but the fault identification indicates no fault situation, there is a high probability that the neural network has a delay in generating the fault identification in this specific scenario, thus assume that the fault in the inductor current sensor occurred and feed the controller with the state of inductor current estimator. When the identification is ready, this condition will not be necessary. The time delays for nominal conditions and the four types of faults can be seen in Table 2.

Table 2. Classification delays

Fault Label	Time delay (ms)	Fault Label	Time delay (ms)
ILOP	10	VCOP	7
ILHG	147	VCHG	0

4. SIMULATION RESULTS

For the evaluation of the neural network performance in classification, a confusion matrix is shown in Figure 3. The

results represent the best performance of 20 trainings using the test set.

Figure 3. Confusion matrix for P_{rnn}.Rows corresponds to the true class (Target Class) accordingly to the Table 1 and Output Class represents the actual predicted output. Both the number of observations and the percentage of the total number of observations are shown in each cell. The last column illustrates the percentage of examples predicted correctly (in green) and incorrectly (in red) for each class. Elements in off-diagonal correspond to examples predicted in the wrong target class. The overall performance is 99, 42% which means that the network can classify the faults situations very well.

To evaluate the reconfiguration strategy, four conditions of fault were tested: inductor current open sensor fault and high gain fault, capacitor voltage open sensor fault and high gain fault, that is represented by Figures 4, 5, 6, 7, respectively. The softwares Matlab™ and Simulink™ were used, with a variable step size and 'ode45' solver with the following parameters for fault simulation: $R_o = 100\Omega, V_{in} = 190V, R = 0.082\Omega, C = 2.85mF, L = 5mH, \rho = 5, x_e = [\,7.6251\ 380\,]'$ and the matrices:

$$G = 10^5 \begin{bmatrix} 1.4025 & 0.1162 \\ -0.0493 & -0.0032 \\ 0 & 0 \\ 0 & 0 \end{bmatrix} \quad F = \begin{bmatrix} 0.9073 & 0.0637 \\ 0.0637 & 0.8591 \end{bmatrix}$$

$$K_g = [\,0.80\ 8\,] \quad K_{int} = [\,0\ 2.3\,]$$

$$L_{est_1} = 10^6\,[\,1.5944\ 0.0662\,]', L_{est_2} = [\,61200\ 1\,]'$$

$$P = \begin{bmatrix} 0.0000 & 0.0001 & -0.0000 & -0.0000 \\ 0.0001 & 0.0038 & -0.0010 & -0.0002 \\ -0.0000 & -0.0010 & 0.9073 & 0.0637 \\ -0.0000- & 0.0002 & 0.0637 & 0.8591 \end{bmatrix}$$

$$\mathscr{S} = [\,0.0000\ 0.0004\ 1.2072\ 1.2448\,]'.$$

The faults occur in 0.60s and the capacitor voltage with reconfiguration and no reconfiguration were represented and compared. A set of two redundant sensors for current and voltage measurement were implemented, since for voltage sensor faults it would be impossible to make any conclusion with the broken sensor.

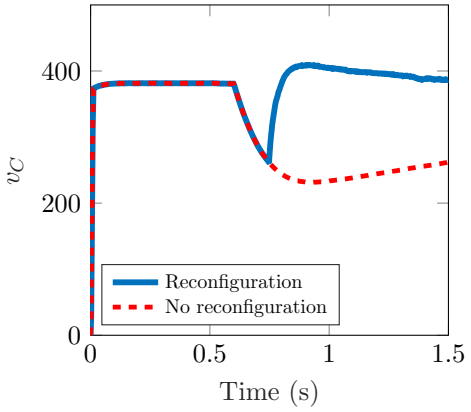

Figure 4. Capacitor Voltage for **ILOP**.

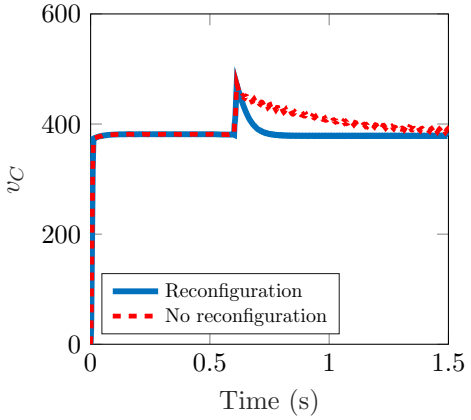

Figure 5. Capacitor Voltage for **ILHG**.

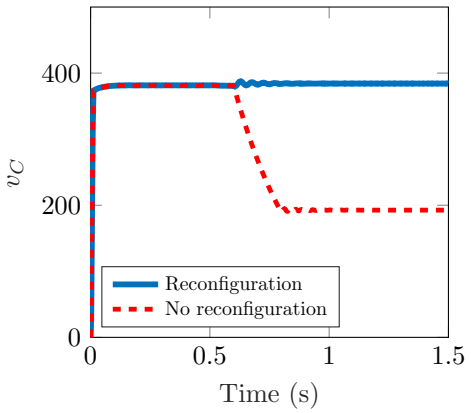

Figure 6. Capacitor voltage for **VCOP**.

In extreme situations of faults in the voltage sensor, the system has a poor performance after the open fault and high gain fault leads the system to instability without a reconfiguration strategy. On the other hand, for all faults simulated, the reconfiguration proved to be very satisfactory in terms of system performance and reliably, with the benefit of taking measurements of the well functioning sensor, which makes possible to detect uncertainties after a fault situation. In addition, the fault detection and identification stage can detect if the fault sensor was fixed.

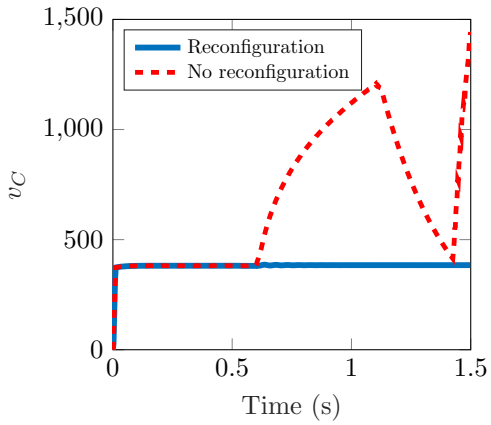

Figure 7. Capacitor voltage for **VCHG**.

5. CONCLUSION

The fault detection observer with a fault identification neural network makes it possible to identify four different faults situations with 99.42%. The reconfiguration strategy worked very well and could maintain the stability and performance in the presence of all faults scenarios. In future works, uncertainties can be considered in the observer design to improve performance.

REFERENCES

Bento, F. and Cardoso, A.J.M. (2018). A comprehensive survey on fault diagnosis and fault tolerance of DC-DC converters. *Chinese Journal of Electrical Engineering*, 4(3), 1–12.

Chaturvedi, S., Fulwani, D., and Patel, D. (2021). Dynamic virtual impedance based second order ripple regulation in dc microgrids. *IEEE Journal of Emerging and Selected Topics in Power Electronics*, 1–1.

Deaecto, G.S., Geromel, J.C., Garcia, F.S., and Pomilio, J.A. (2010). Switched affine systems control design with application to DC–DC converters. *IET Control Theory Applications*, 4(7), 1201–1210.

Espinoza-Trejo, D.R., Diez, E., Barcenas, E., Verde, C., Espinosa-Pérez, G., and Bossio, G. (2016). Model-based fault detection and isolation in a mppt boost converter for photovoltaic systems. In *IECON 2016-42nd Annual Conference of the IEEE Industrial Electronics Society*, 2189–2194. IEEE.

Ferreira Costa, L. and Liserre, M. (2018). Failure analysis of the DC-DC converter: A comprehensive survey of faults and solutions for improving reliability. *IEEE Power Electronics Magazine*, 5(4), 42–51.

Givi, H., Farjah, E., and Ghanbari, T. (2017). Switch and diode fault diagnosis in nonisolated DC–DC converters using diode voltage signature. *IEEE Transactions on Industrial Electronics*, 65(2), 1606–1615.

Hwang, I., Kim, S., Kim, Y., and Seah, C.E. (2009). A survey of fault detection, isolation, and reconfiguration methods. *IEEE transactions on control systems technology*, 18(3), 636–653.

Ivanovic, Z., Blanusa, B., and Knezic, M. (2014). Analytical power losses model of boost rectifier. *IET Power Electronics*, 7(8), 2093–2102.

Komurcugil, H., Biricik, S., and Guler, N. (2020). Indirect sliding mode control for dc–dc sepic converters. *IEEE Transactions on Industrial Informatics*, 16(6), 4099–4108.

Li, J., Pan, K., and Su, Q. (2019). Sensor fault detection and estimation for switched power electronics systems based on sliding mode observer. *Applied Mathematics and Computation*, 353, 282–294.

Li, J., Zhang, Z., and Li, B. (2018). Sensor fault detection and system reconfiguration for DC-DC boost converter. *Sensors*, 18(5), 1375.

Magossi, R.F.Q., Elias, L.J., Faria, F.A., Machado, R.Q., and Oliveira, V.A. (2021). A n-PWM DC-DC converter modeling: Switched systems meets Fourier series. *IEEE Transactions on Industrial Electronics*, 1–1.

Magossi, R.F.Q., Han, S., Machado, R.Q., Oliveira, V.A., and Bhattacharyya, S.P. (2020). Geometric-based PID control design with selective harmonic mitigation for DC–DC converters by imposing a norm bound on the sensitivity function. *IET Control Theory & Applications*.

Martinez-Treviño, B.A., El Aroudi, A., Vidal-Idiarte, E., Cid-Pastor, A., and Martinez-Salamero, L. (2019). Sliding-mode control of a boost converter under constant power loading conditions. *IET Power Electronics*, 12(3), 521–529.

Shtessel, Y., Edwards, C., Fridman, L., and Levant, A. (2014). *Sliding mode control and observation*, volume 10. Springer.

Silveira, A.M. and Araújo, R.E. (2020). A new approach for the diagnosis of different types of faults in DC–DC power converters based on inversion method. *Electric Power Systems Research*, 180, 106103.

Slotine, J.J.E., Li, W., et al. (1991). *Applied nonlinear control*, volume 199. Prentice hall Englewood Cliffs, NJ.

Tarzamni, H., Esmaeelnia, F.P., Tahami, F., Fotuhi-Firuzabad, M., Dehghanian, P., Lehtonen, M., and Blaabjerg, F. (2021). Reliability assessment of conventional isolated PWM DC-DC converters. *IEEE Access*, 9, 46191–46200.

Utkin, V. (2013). Sliding mode control of DC-DC converters. *Journal of the Franklin Institute*, 350(8), 2146–2165.

Utkin, V., Poznyak, A., Orlov, Y., and Polyakov, A. (2020). Conventional and high order sliding mode control. *Journal of the Franklin Institute*, 357(15), 10244–10261.

Vázquez, N., Leyva, J., Cervantes, I., Diaz, L., and Hernández, C. (2013). Analysis and study of high dc/dc boost converters. In *IECON 2013 - 39th Annual Conference of the IEEE Industrial Electronics Society*, 435–440.

Yao, B., Chen, H., He, X.Q., Xiao, Q.Z., and Kuang, X.J. (2013). Reliability and failure analysis of DC/DC converter and case studies. In *2013 International Conference on Quality, Reliability, Risk, Maintenance, and Safety Engineering (QR2MSE)*, 1133–1135.

Yazici, I. and Yaylaci, E.K. (2016). Fast and robust voltage control of dc–dc boost converter by using fast terminal sliding mode controller. *IET Power Electronics*, 9(1), 120–125.

Zhao, Y., Wang, J., Yan, F., and Shen, Y. (2019). Adaptive sliding mode fault-tolerant control for type-2 fuzzy systems with distributed delays. *Information Sciences*, 473, 227–238.